JOURNAL OF SOLID STATE CHEMISTRY **141,** 527–536 (1998)
ARTICLE NO. SC988015

Hydrothermal Synthesis, Crystal Structure, and Properties of $CuAl_2Si_2O_7(F,OH)_2$

Petr E. Izokh,* Werner Joswig,†,[1] Dmitry A. Fursenko,* Alexandra V. Leont'eva,* Sergei V. Vosel,* Victor G. Thomas,* and Boris A. Fursenko*

*Institute of Mineralogy and Petrography, Russian Academy of Sciences, 630090 Novosibirsk, Russia; and †Institute of Mineralogy, Frankfurt University, D-60054 Frankfurt am Main, Germany

Received February 7, 1997; in revised form August 17, 1998; accepted August 27, 1998

A new copper aluminum silicate $CuAl_2Si_2O_7(F,OH)_2$ (cualsite) was synthesized hydrothermally from SiO_2 and Al_2O_3 in a mineralizing solution $\frac{1}{3}Na_3AlF_6 + \frac{4}{9}Al(NO_3)_3 + \frac{1}{9}Cu(NO_3)_2 + 27.8H_2O$ at 600°C and 150 MPa. Cualsite grew epitaxially on the pinacoidal plane of the topaz single-crystal seed. Blue crystals of the bipyramidal habitus exhibit orthorhombic symmetry *Pbnm* with $a = 4.757(1)$ Å, $b = 8.877(3)$ Å, $c = 14.075(4)$ Å, and $Z = 4$. Structural analysis led to $R_1 = 0.018$ and $R_w = 0.046$ for 899 unique reflections. The cualsite structure was shown to be in close relation with that of topaz and may be represented (perpendicular to the *c* axis) as a sandwich of topaz layered fragments and ($CuSiO_3$) layers. Copper has a (4+1) square-pyramidal coordination, with the vertex oxygen being a bridging oxygen of an isolated [Si_2O_7] diortho group. Inside one layer, [CuO_4] squares separated by [Si_2O_7] diortho groups form a zigzag chain with an angle of 103°. The ESR spectrum of interacting Cu^{2+} ions in cualsite coincides well with this arrangement. Full identity between the cualsite and topaz structures in the *ab* plane explains well the epitaxial growth of cualsite on the topaz single-crystal seeds. A comparison is made of the cualsite structure and other known copper silicates. © 1998 Academic Press

INTRODUCTION

Only a few silicate compounds containing divalent Cu as a main component are known. In addition to the more or less common mineral dioptase, there are the rare minerals plancheite and shattuckite (1) synthesized hydrothermally in (2), kinoite (3), litidionite (4), papagoite ($CaCuAlSi_2O_6(OH)_3$) (5), and some synthetic compounds (6, 7). At the same time, the Cu^{2+} ion is well known by its paramagnetic character and chromophore properties (blue and green color of many minerals). The special role of the Cu^{2+} ion in high-temperature superconductors has also been attracting attention to the copper oxide compounds (8).

[1]To whom correspondence should be addressed. E-mail: joswig@kristall.uni-frankfurt.d400.de.

We have introduced the Cu^{2+} ion into the system, as a coloring agent when studying topaz crystal growth in hydrothermal conditions. Light-blue crystalline material has been grown on topaz single crystals during experiments. It was shown to be a new Cu^{2+}-containing compound with a composition close to $CuAl_2Si_2O_7(F,OH)_2$. The name *cualsite* (from the main cations: Cu, Al, and Si) used herein to designate this phase is a working term only, because no such mineral has been found in nature yet. In this paper we present experimental data on the growth conditions of cualsite, its crystal structure, and some physical properties, with emphasis on ESR spectroscopy, which is very informative in the case of the paramagnetic Cu^{2+} ion.

EXPERIMENTAL

Hydrothermal Synthesis

Experiments were conducted in steel autoclaves (volume 200 ml) at the average temperature $T_{av} = (T_{bot} + T_{top})/2 = 600 \pm 1$°C and pressure about 150 MPa (as given by filling coefficients equal to 0.5). The temperature gradient along the autoclave was $\Delta T = T_{bot} - T_{top} = 80$–$100$°C. Both T_{bot} and T_{top} were measured by two chromel–alumel thermocouples positioned about 5 mm away from the inner wall of the autoclave in the bottom part and in the obturator, respectively. The principal arrangement of the charge material, seeds, and diaphragm was nearly the same in all runs and is shown in Fig. 1.

All charge material was placed in a metallic net container in the lower part of the autoclave. The frame with the seeds was placed in the upper part of the autoclave. A 10% perforated diaphragm was positioned in the middle of the autoclave (at about half height). Thin plates of topaz single crystals cut parallel to the basic pinacoid plane were used as the seeds. The charge was a mixture of silica (natural quartz (SiO_2)) and alumina (fused electrocorundum (Al_2O_3)). Typical run duration was 1–2 weeks.

0022-4596/98 $25.00

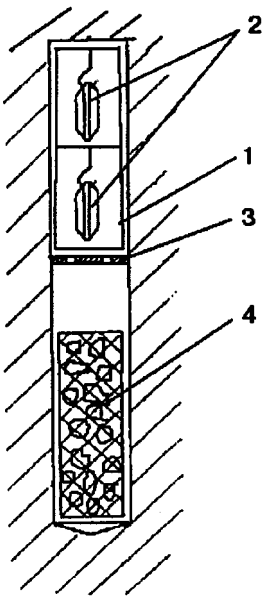

FIG. 1. Schematic representation of hydrothermal experiment: (1) frame; (2) single-crystal seeds; (3) diaphragm; (4) net with the charge.

Cualsite synthesis was carried out in alkaline fluoride solutions of complex composition. The following solution was used as the main mineralizing agent:

$$\tfrac{1}{3}Na_3AlF_6 + \tfrac{4}{9}Al(NO_3)_3 + \tfrac{1}{9}Cu(NO_3)_2 + 27.8H_2O.$$

Concentrations are given in moles per liter of the free autoclave volume (the free volume being equal to the total volume minus the volume of the solid charge and armature). The presence of an oxidative agent (NO^{3-} in this particular case) ensured that copper was in the divalent state, the same oxidation state as in cualsite. The above composition was changed slightly in some cases: the Cu content was varied and some minor admixtures were added to the charge (e.g., V_2O_3).

Sample Characterization

Goniometric study was conducted on a ZRG-3 two-limb reflection goniometer (Germany). Well-shaped spontaneous crystals up to 1 mm were chosen for the measurements. Crystals were mounted parallel to the elongation. Orthorhombic bipyramid faces were used for crystal alignment (Fig. 2).

The chemical composition of the synthesized material was determined by an electron microprobe (Cambex-Micro). Kyanite, fluorphologopite, and tenorite were used as standards for the electron microprobe analysis. The chemical compositions of the pure and V-containing cualsite as well as of natural and synthetic topaz are presented in Table 1.

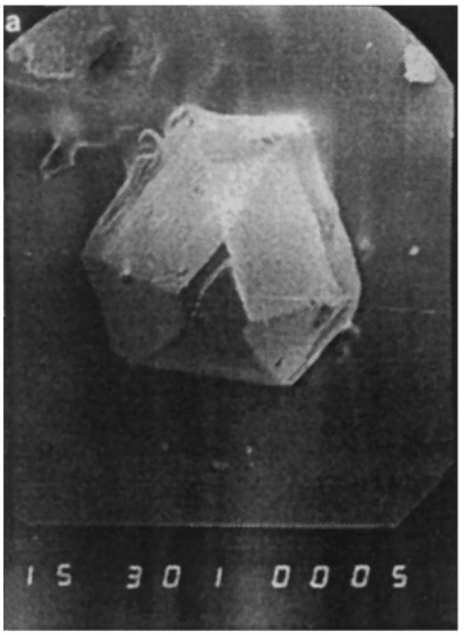

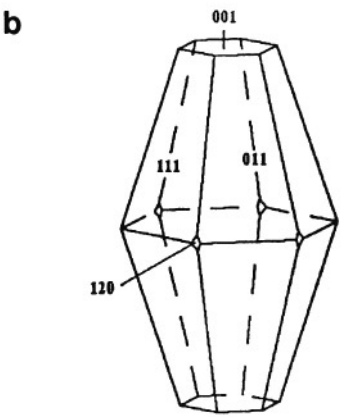

FIG. 2. Cualsite single crystals: (a) scanning microscope photograph (crystal size is about 1 mm); (b) schematical drawing of the bipyramidal spontaneous crystal.

X-ray powder diffraction data were collected on a DRON-3 powder diffractometer with CuKα radiation and a graphite monochromator. Al_2O_3 powder was used as an internal standard. Measured d/n and relative intensities are summarized in Table 2.

The IR spectrum of cualsite was registered on a Specord IR spectrometer (Germany). ESR study was conducted at room temperature with a JES-3BX ESR spectrometer (Japan). g-factor values were determined by comparison with an external standard (DPPH).

High-temperature behavior and decomposition above 1000°C were studied by thermogravimetry and thermoanalysis on an OD-102 derivatograph (Hungary).

TABLE 1
Electron Microprobe Analysis of Cualsite and Topaz

Oxide	Composition (wt%)[a]			
	Cualsite, blue	Cualsite, green	Synthetic topaz	Natural topaz[b]
SiO_2	36.42	35.89	30.22	31.03
Al_2O_3	30.98	30.65	54.55	52.47
CuO	23.66	23.04	0.07	—
Cr_2O_3	—	Trace	Trace	—
V_2O_3	Trace	0.26	Trace	—
FeO	0.14	0.11	0.11	0.08
F[a]	8.18	8.23	14.23	14.85
Sum	99.38	98.18	99.18	98.43
$-O = F_2$	3.44	3.46	5.99	6.25
Sum	95.94	94.71	93.19	92.18
Unit cell parameter b (Å)	8.877(3)	8.873(4)	8.820(3)	8.820(3)
F[c]	9.67[c]	9.73[c]	17.56[d]	17.56[d]
	Atomic quantities per formula unit			
Si	2.003	2.000	0.958	1.002
Al	2.008	2.013	2.038	1.996
Cu	0.983	0.970	0.002	0
V^{3+}	0	0.012	0	0
Fe^{2+}	0.006	0.005	0.003	0.002
F[a]	1.423	1.450	1.426	1.516
F[c]	1.67	1.69	1.76	1.79
OH[e]	0.38	0.36	0.19	0.22

[a] As an average value of five measurements in different places of a sample.
[b] The seed material (cf. Fig. 1).
[c] As estimated by assuming the same error level as in topaz.
[d] F wt% = 892.5–99.2b (17).
[e] As determined from cation–anion charge balance.

TABLE 2
X-Ray Powder Diffraction Data of Cualsite

I/I_0	d_{exp} (Å)	$2\theta_{exp}$	$2\theta_{calc}$	$\Delta 2\theta^*_{calc}$	hkl
7	4.5020	19.72	19.702	+0.018	101
6	4.4396	20.00	20.006	−0.006	020
11	4.2304	21.00	20.988	+0.012	021
100	4.0186	22.12	22.124	−0.004	111
5	3.7542	23.70	23.701	−0.001	022
10	3.6016	24.72	24.719	+0.001	112
6	3.5203	25.30	25.312	−0.012	004
5	3.3413	26.68	26.690	−0.010	103
63	3.2435	27.50	27.488	+0.012	120
9	3.1623	28.22	28.223	−0.003	121
7	2.9470	30.33	30.332	−0.002	122
10	2.7575	32.47	32.473	−0.003	024
53	2.6945	33.25	33.242	+0.008	114
10	2.5123	35.74	35.740	0.000	130
5	2.4748	36.30	36.324	−0.024	131
8	2.4220	37.12	37.113	+0.007	105
42	2.3776	37.84	37.848	−0.008	025
14	2.2671	39.76	39.759	+0.001	211
6	2.1850	41.32	41.346	−0.026	212
23	2.1261	42.52	42.515	+0.005	125
11	2.0965	43.15	43.157	−0.007	220
24	2.0474	44.24	44.245	−0.005	116
3	2.0111	45.08	45.084	−0.004	140
6	1.9902	45.58	45.567	+0.013	141
14	1.9226	47.28	47.255	+0.025	214
3	1.9006	47.86	47.848	+0.012	126
8	1.8745	48.57	48.573	−0.003	135

Single-Crystal Structure Determination

Several cualsite crystals were checked by Laue photographs, and a green (V-containing) specimen shaped as an equilateral triangle (0.45-mm length and 0.1-mm thickness) was chosen for the experiment. The data collection was performed at room temperature on a single-crystal diffractometer (Enraf-Nonius CAD4) with Mo$K\alpha$ radiation applying the ω-scan method (altogether ca. 2900 intensities were measured over the half sphere of reflection).

Due to the absorption coefficient and the shape of the crystal, an experimental absorption correction (ψ-scan technique) was carried out. The background corrections were determined by profile analysis (9).

The lattice constants were refined by 25 reflections ($23^\circ < 2\theta < 45^\circ$) with positive and negative 2θ determination. The crystal and experimental data together with the refinement data are given in Table 3.

The extinction rules indicate the centrosymmetric space group *Pbnm* (No. 62) and the noncentrosymmetric space group $Pbn2_1$ (No. 33). As piezoelectric data (Dr. V. A. Gritchin, personal communication) show centrosymmetry, the space group *Pbnm* was taken for the structure determination by direct methods: SHELXS-90 (10).

TABLE 3
Crystal Data and Experimental Parameters

Chemical formula	$CuAl_2Si_2O_7F_2$
Crystal system	Orthorhombic
Space group	*Pbnm* (No. 62)
a (Å)	4.7602(4)
b (Å)	8.8766(10)
c (Å)	14.0923(12)
V (Å^3)	595.5
Z	4
D_x (Mg m^{-3})	3.61
Scan	ω
λ(Mo$K\alpha$) (Å)	0.7107
$(\sin\theta/\lambda)_{max}$ (Å^{-1})	0.7
μ(Mo$K\alpha$) (mm^{-1})	4.43
Size of crystal (μm)	450/100
Number of I_{hkl} measured	2838
Number of I_{hkl} (averaged) (NREF)	899
h_{min}, h_{max}, k_{min}, k_{max}, l_{min}, l_{max}	−6,6, 0,12, −19,19
Number of variables (NVAR)	71
$R_1 = R(F) = \sum[\lvert F_o\rvert - \lvert F_c\rvert]\sum\lvert F_o\rvert$	0.018
$wR_2 = R(wF^2) = [\sum w(F_o^2 - F_c^2)^2/\sum w(F_o^2)^2]^{1/2}$	0.046
GoF = $[\sum w(F_o^2 - F_c^2)^2/(\text{NREF} - \text{NVAR})]^{1/2}$	1.14

TABLE 4
Atomic Positions, Displacement Parameters, and Population Factors of Cualsite

Atom	*x*	*y*	*z*	*U*(eq) (Å)	Population
Cu	0.13262(5)	0.85802(3)	0.75	0.00548(9)	0.940(2)
Si	−0.09579(7)	0.56185(4)	0.64628(2)	0.00344(14)	0.948(4)
Al	0.09625(8)	0.86853(4)	0.54954(3)	0.00377(14)	0.955(3)
F	−0.10431(16)	0.75326(9)	0.46858(6)	0.00860(23)	0.979(4)
O(1)	−0.03275(21)	0.74284(11)	0.64664(6)	0.00768(22)	1
O(2)	0.30415(21)	0.96589(11)	0.85614(6)	0.00794(22)	1
O(3)	−0.30080(19)	0.51306(10)	0.55819(7)	0.00712(21)	1
O(4)	−0.24459(31)	0.52461(15)	0.75	0.00816(27)	1

TABLE 5
Interatomic Distances (Å) and Angles (deg) in Cualsite and Topaz (13)

CuO pyramid			AlO_4F_2 octahedron		
Cualsite			Cualsite		Topaz
Cu–O(1) [×2]	1.946(1)		Al–F	1.807(1)	1.790
Cu–O(2) [×2]	1.955		Al–F′	1.804	1.790
Mean	1.950		Mean	1.806	1.795
Cu–O(4)	2.366(1)		Al–O(1)	1.869(1)	1.901
O(1)–O(2) [×2]	2.547(1)	81.58(4)	Al–O(2)	1.870	1.896
O(1)–O(1)	2.914	96.93(6)	Al–O(3)	1.910	1.884
O(2)–O(2)	2.990	99.85(6)	Al—O(3′)	1.908	1.897
O(1)–O(4)	3.083	90.72(4)	Mean	1.889	1.8945
O(2)–O(4)	3.098	91.13(4)	F–F′	2.540(1)	2.516
			F–O(1)	2.607	2.626
			F–O(2)	2.548	2.573
SiO_4 tetrahedron			F–O(3)	2.649	2.625
			F′–O(1)	2.533	2.592
	Cualsite	Topaz	F′–O(3)	2.555	2.547
			F′–O(3′)	2.668	2.645
Si–O(1)	1.634(1)	1.644	Mean	2.593	2.601
Si–O(2)	1.629	1.636	O(1)–O(2)	2.549(1)	2.525
Si–O(3)	1.637	1.642 ×2	O(1)–O(3′)	2.817	2.806
Si–O(4)	1.657		O(2)–O(3)	2.898	2.904
Mean	1.639	1.641	O(2)–O(3′)	2.716	2.730
O(1)–O(2)	2.689(1)	2.685	O(3)–O(3′)	2.518	2.503
O(1)–O(3)	2.709	2.697 ×2	Mean	2.633	2.633
O(1)–O(4)	2.625				
O(2)–O(3)	2.68	2.675 ×2			
O(2)–O(4)	2.628				
O(3)–O(4)	2.718	2.650	F–Al-F′	89.35(2)	89.0
Mean	2.676	2.680	F–Al–O(1)	90.32(3)	90.7
			F–Al–O(2)	87.68(4)	88.5
			F–Al–O(3)	90.83(4)	91.2
			F′–Al–O(1)	87.16(4)	88.9
O(1)–Si–O(2)	110.95(6)	109.9	F′–Al–O(3)	86.88(4)	87.4
O(1)–Si–O(3)	111.80(5)	110.3 ×2	F′–Al–O(3′)	91.84(4)	91.3
O(1)–Si–O(4)	105.77(6)	107.5	O(1)–Al–O(2)	85.95(4)	83.4
O(2)–Si–O(3)	110.72(5)	109.4 ×2	O(1)–Al–O(3″)	96.50(5)	95.2
O(2)–Si–O(4)	106.16(6)		O(2)–Al–O(3)	100.10(4)	100.4
O(2)–Si–O(4)	111.16(6)		O(2)–Al–O(3′)	91.91(4)	92.1
Mean	109.43	109.5	O(3)–Al–O(3′)	82.54(4)	82.9

The structure determination shows that cualsite belongs to the sorosilicate group; the double tetrahedra are linked by Al octahedra and Cu polyhedra. For the following refinement calculations by SHELXL-93 (11), the data set was averaged, resulting in 899 unique intensities ($R_{int} = 1.28\%$). After refinement of the positional and displacement parameters as well as the site occupancy factors of the cation and fluorine, the final *R* value converged to 1.8%, including all intensities (no σ limit). Positional and displacement parameters are given in Table 4, and interatomic distances and angles in Table 5.

RESULTS

Hydrothermal Synthesis of $CuAl_2Si_2O_7(F,OH)_2$

Cualsite grew epitaxially on the basal pinacoid surface of the topaz single-crystal seed. The average growth rate was 0.1–0.2 mm/day. No growth of cualsite was observed when seeds were cut along other directions. If the seed surface was not exactly but close enough to the (001) plane, separate subindividual cualsite units began to grow initially. Then they became larger and coalesced into one layer. The spherical topaz seed became almost completely well shaped by the cualsite crystal faces except for a narrow band at the prism zone.These facts allow us to conclude that the only direction where an epitaxial growth of cualsite on topaz can occur is a basal pinacoid plane.

When cualsite was grown under copper-deficient conditions, the growth layers became inhomogenous. Formation of a "sandwich" of interchanged layers of cualsite and topaz composition was observed. Further reduction of copper content in the system led to formation of small (<100 μm) flat cualsite clusters in topaz. The lower the Cu content was, the sparser these cualsite clusters were. The electron microprobe profiles presented in Fig. 4 demonstrate this situation.

The observed intergrowth of cualsite and topaz can be attributed to the absence of isomorphic miscibility between these compounds and the impossibility of Cu^{2+} incorporation into the topaz structure. In this case, topaz will crystallize at low copper concentration, while the diffusion zone around the seed will be enriched in copper. After the critical Cu concentration is achieved, it will be released by forming of a new cualsite layer (or cualsite clusters) and a new cycle will begin.

The isomorphic capacity of topaz is known to be low (12). The same was confirmed by our attempts to introduce some 3*d* elements into topaz. The concentration of these elements in topaz never exceeded a few hundredths of a percent. In this connection, it was of interest to check the isomorphic capacity of cualsite. V^{3+} was introduced into the system in the form of sesquioxide V_2O_3. Grass-green cualsite crystals grew under these conditions. They contained about 0.3 wt% of V_2O_3 (Table 1). It should be mentioned that under our experimental conditions (high NO_3 concentration) the stable vanadium phase was V_2O_5; hence the V^{3+} concentration in

solution was very low. Nevertheless its concentration in cualsite was relatively high.

In all runs, accompanying phases were synthesized on the seeds along with cualsite: first topaz in the form of small (< 0.1 mm) spontaneous crystals and then cryolite (Na_3AlF_6) in the form of large (up to 1 mm) spontaneous crystals. Cualsite spontaneous crystals were observed in some runs, too. They were mostly of elongated pseudohexapyramidal habit (Fig. 2a) and more rarely of pseudobipyramidal habit (Fig. 2b). Often these crystals were grown on topaz.

Crystal Morphology

As evidenced from our goniometric study, the following crystal faces are usually developed on the cualsite crystals (Fig. 2): orthorhombic bipyramid (111) and orthorhombic prism (011). The orthorhombic prism (120) and pinacoid (001) are also present on some crystals.

X-Ray Powder Diffraction and Unit Cell Parameters

The X-ray powder diffraction pattern of cualsite (Table 2) was indexed successfully in the orthorhombic unit cell (space group *Pbnm*). The following cell parameters were calculated by routine least-squares procedure: $a = 4.757(1)$ Å, $b = 8.877(3)$ Å, $c = 14.075(4)$ Å, $V = 594.4(2)$ Å^3, $Z = 4$. It is noteworty that the a and b parameters of cualsite are very close to those of topaz ($a = 4.660(1)$ Å, $b = 8.820(3)$ Å), whereas, the c parameter is significantly larger ($c = 8.400(4)$ Å in topaz).

Physical Properties

Cualsite formed transparent blue crystals with a vitreous luster. The V-doped crystals were green and very brittle. The {001} cleavage is perfect. The X-ray density is 3.48–3.49 g/cm^3. Mohs hardness is 7 and the microhardness (Wickers) is 1120(50) kg/mm^2. The optical properties are $n_p = 1.625$, $n_m = 1.644$, $n_g = 1.668$, $n_g - n_p = 0.043$, and $2V = 82°$. Direct measurement of the piezoelectric effect (Dr. V. A. Gritchin, NSTU, Novosibirsk) showed its absence, indicating the crystal to be centrosymmetric.

Chemical Composition

The chemical compositions of pure and V-containing cualsite are presented in Table 1 together with those of synthetically grown topaz and natural topaz used as a seed. Synthetic topaz analysis corresponds to the run where topaz layers were interchanged with cualsite ones.

It is known that microprobe analysis can underestimate fluorine content. This seems to be the case with our cualsite and topaz analyses, the low sum being one of the manifestations of this. Another indication is the low values of F determined for topaz: 14.85–14.23 wt%, which correspond to 1.52–1.43 atoms per formula unit. This is too low for the synthesis conditions and is in strong disagreement with other observed properties of our topaz samples. Thus an estimation by the well-established correlation of the F content and topaz unit cell parameter b (17) gives a more reasonable value: about 17.56 wt% (1.7 atoms per formula unit) for both natural and synthetic topaz ($b = 8.820(3)$ Å)

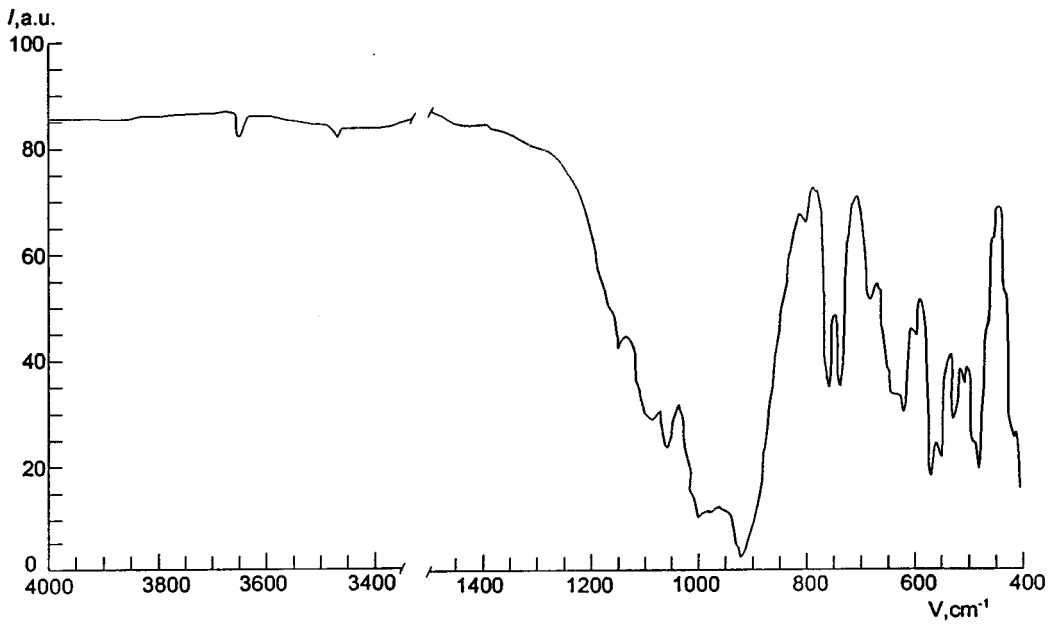

FIG. 3. Cualsite IR spectrum. The small peak near 3700 cm^{-1} corresponds to OH group vibrations.

(Table 1). Assuming approximately the same error level in cualsite microprobe analyses, we estimate its F content as 9.6 wt%, or 1.7 atoms per formula unit. This value is in satisfactory agreement with that derived from the thermogravimetry curve of cualsite (see next section), which gives 1.86 fluorine atoms per formula unit. The relatively low amount of OH groups in cualsite was revealed by IR spectroscopy (see low-intensity peak near 3650 cm^{-1} in Fig. 3). Taking into account all of the above, we can write the following chemical formula for the particular cualsite: $Cu_{0.98}Al_{2.01}Si_{2.00}O_7(F_{0.9}OH_{0.1})_2$, or in generalized form $CuAl_2Si_2O_7$ $(F,OH)_2$.

Surprising results were obtained for the "sandwich" samples, where an interchange of deep blue and colorless zones was visually observed. The microprobe profiles of the main components taken across such a sample (along the growth direction) are presented in Fig. 4. An increase in CuO content is distinctly seen in the blue zone, which has well-defined sharp boundaries. However, the CuO content in this zone does not exceed 1.5 wt%, whereas in stoichiometric cualsite this value must be one order higher. The same low CuO content was detected in other points along this zone. To explain this observation one can assume the presence of very thin microlayers of cualsite and topaz in the blue zones. If so, these microlayers have to be smaller than the microprobe electron beam diameter (about 3 μm). The reasons for and possibility of such thin interlayer formation will be discussed shortly.

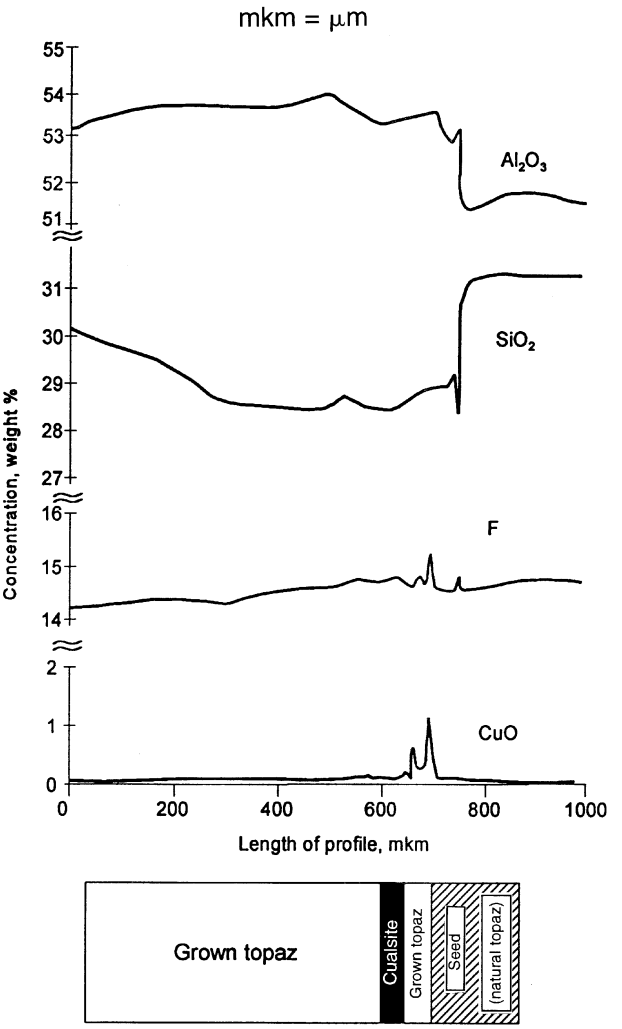

FIG. 4. Electron microprobe profiles through the single-crystal topaz seed with synthetic topaz and cualsite layers (see text for details).

Thermal Behavior

Two endothermic effects were observed in cualsite when it was heated to 1300°C (Fig. 5). The second one, at 1000°C, is due to cualsite decomposition and is accompanied by a 15.36% weight loss. The decomposition products (after 1300°C) were mullite ($Al_6Si_2O_{13}$) and tenorite (CuO) as revealed by X-ray powder diffraction. No SiO_2 crystalline phases were detected by X-ray powder diffraction. However, a high background level was observed, indicating the presence of an amorphous phase.

By analogy with topaz decomposition, one can assume the following reaction:

$$6CuAl_2Si_2O_7F_{2x}(OH)_{2(1-x)} = 6CuO + 2Al_6Si_2O_{13} + (8-3x)SiO_2 + 3xSiF_4 + 6(1-x)H_2O.$$

The resulting weight loss calculated from this equation for $x = 0.85$ is 14.53%, which is lower than the measured value of 15.36%. On the other hand, one can calculate x from the weight loss value. The thus obtained x value is 0.93, being another reasonable estimation of the fluorine content in our sample (see above).

Description of the Structure

The crystal structure of cualsite (Fig. 6) can be described by analogy with that of topaz. The interrelation between the structures is shown in Fig. 7. The main building elements of both structures are $[AlO_4F_2]$ octahedra and $[SiO_4]$ tetrahedra. However, the key unit of the topaz structure is the crankshaft chain of edge-sharing $[AlO_4F_2]$ octahedra and corner-sharing $[SiO_4]$ tetrahedra running parallel to z (Fig. 7a) (13), whereas in cualsite this unit is broken along the common octahedral edge and an extra $[SiO_4]$ tetrahedron is fitted into the chain, forming a $[Si_2O_7]$ diortho group (Figs. 7c and 7d). Copper atoms are situated between these two shifted octahedra in the plane of their previously shared edges. As a result, the c parameter of the cualsite lattice becomes more than 1.5 times larger than that of topaz. One can easily calculate a theoretical value of c, which is equal

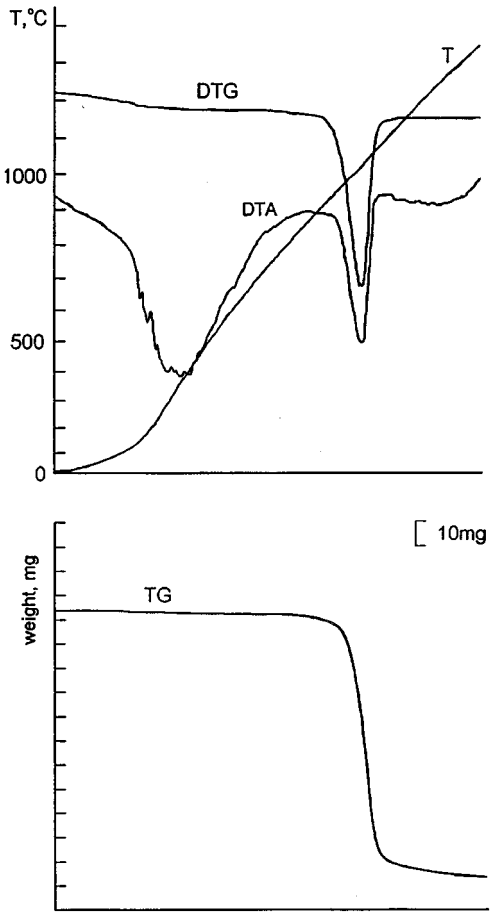

FIG. 5. Cualsite derivatogram: TG = weight loss, DTG = derivative of the weight loss, DTA = differential thermal analysis curve, T = sample temperature vs furnace temperature.

to the sum of the topaz c parameter plus two edges of the $[SiO_4]$ tetrahedron (cf. Fig. 7b): $c_{th} = 8.400(4) + 2.650 \times 2 = 13.700$ Å. This value is comparable to the measured c parameter of cualsite, 14.075(4) Å. At the same time, the lattice parameters a and b of both compounds are almost the same: $a = 4.757(1)$ Å and $b = 8.877(3)$ Å for cualsite and $a = 4.660(1)$ Å and $b = 8.820((3)$ Å for topaz. This is due to the full identity of both structures in the ab plane (Figs. 7b and 7e).

Thus, on the one hand, the cualsite structure viewed in the bc plane (Fig. 7d) is very close to the schematic representation built from topaz structural fragments (Figs. 7a and 7c). On the other hand, the cualsite structure can be described as composed from the layered fragments of the topaz structure—octahedral sheets parallel to the ab plane, which are distinctly seen in Fig. 6 and are separated by diortho groups $[Si_2O_7]$ and Cu atoms.

The coordination polyhedra in both structures are almost the same. The interatomic distances and intrapolyhedral

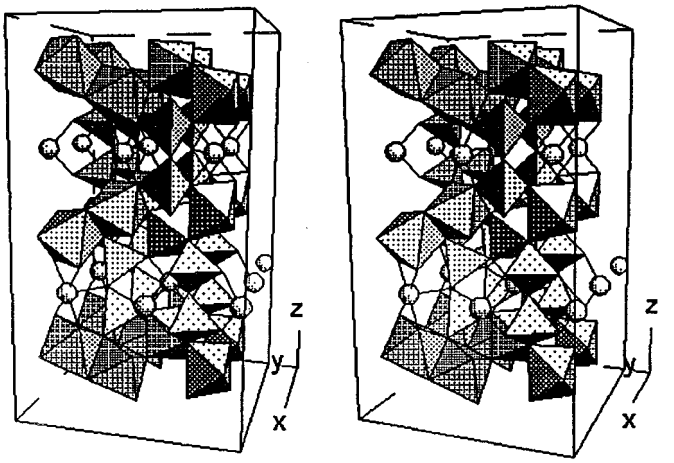

FIG. 6. Stereoview of cualsite structure in polyhedral representation.

angles differ insignificantly (Table 5). One exception is the increase of the O(1)–O(2) distance to 2.549 Å in cualsite compared to 2.525 Å in topaz. However, this is easy to explain because in topaz it is a common edge shared by two Al octahedra and in cualsite it is an edge shared by an Al octahedron and a $[CuO_4]$ square plane (Fig. 8).

Slightly larger Al–(F,OH) distances in cualsite compared to F-topaz (Table 4) may be attributed to partial substitution of OH for F, In topaz, this substitution led directly to an increase in unit cell parameter b. The same must be the

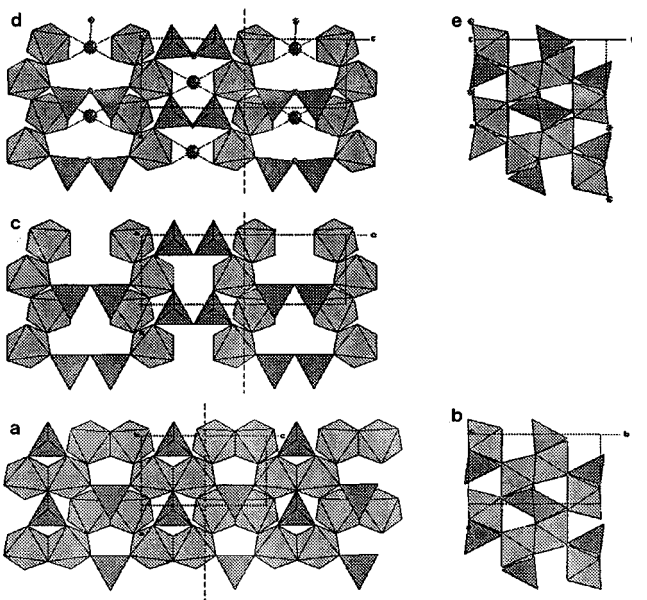

FIG. 7. Interrelation between cualsite and topaz structures: (a) topaz structure projected down y (cf. (13)); (b) disjointed fragments of topaz structure with additional $[SiO_4]$ tetrahedra between them as an ideal cualsite matrix; (c) cualsite structure projected down y; (d, e) projections down z. Dashed lines show the trace of the {001} cleavage (after (13)).

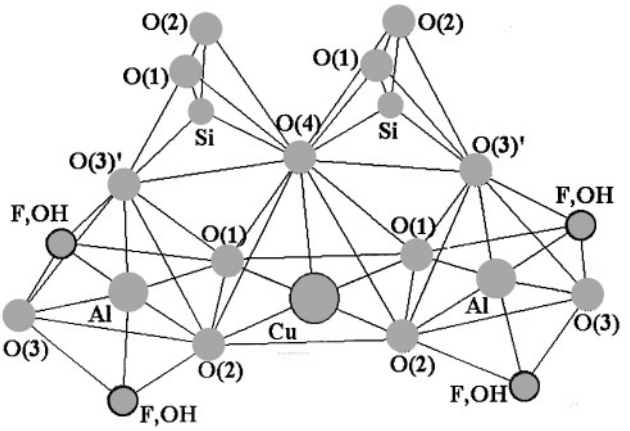

FIG. 8. Main coordination polyhedra of cualsite structure.

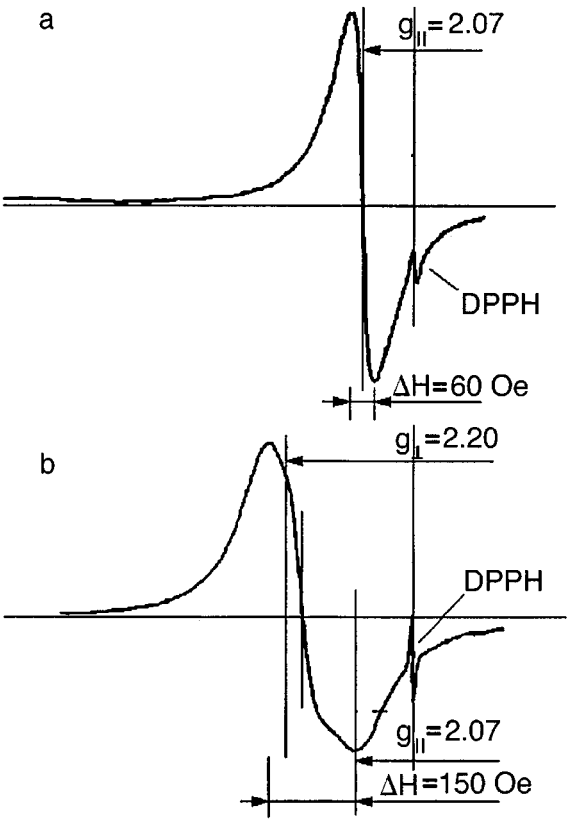

FIG. 9. ESR spectra of cualsite; (a) single crystal; (b) powder sample.

case in cualsite but the picture may be complicated by some deviations from closest packing along the *b* axis.

The $[Si_2O_7]$ diortho group formed in cualsite instead of the single $[SiO_4]$ tetrahedron present in topaz is characterized by a very small $\langle$Si–O–Si$\rangle$ angle (123.7°). This value is far from the average value of this angle (139°) (15) and lies even below the low limit found in diortho groups (128.2° (15)).

The Cu^{2+} coordination can be represented as a pyramidal (4 + 1) coordination (Fig. 8). Four oxygen atoms from the opposite edges of two "shifted apart" octahedra from an almost ideal plane (approximately flat square) in the center of which there is a Cu atom. The average Cu–O distance in this plane is 1.95 Å, which is close to those of other known copper–oxygen compounds. The fifth oxygen has a larger Cu–O distance equal to 2.366 Å. Thus the coordination polyhedron of Cu^{2+} in cualsite is a tetragonal pyramid whose base is composed from two edges of Al octahedra and whose vertex is a central bridging oxygen atom of the $[Si_2O_7]$ diortho group. The latter may be considered as an explanation of the very small Si–O–Si angle in the diortho group. It is known that at higher O coordination the Si–O–Si angle in the diortho group may be lower (15).

Detailed comparison of interatomic distances and angles in cualsite and topaz is presented in Table 5.

Electron Spin Resonance of Cualsite

A cualsite single crystal exhibits a single symmetric ESR line (Fig. 9a), the line width being $\Delta H = 60$ Oe. The line position depends on the crystal orientation in the magnetic field (H_0). When the *c* axis of the crystal is parallel to H_0, the line position corresponds to the *g*-factor value $g_c = 2.07$; when the *ab* plane is parallel to H_0, $g_a = g_b = 2.21$. The observed values of the main *g* tensor components are in correspondence with the ESR spectrum of cualsite powder (Fig. 9b), which is characterized by $g_\parallel = 2.07$, $g_\perp = 2.20$, and line width about 150 Oe.

Numerous ESR studies of Cu ions in various oxide matrices (16) showed that the *g* factor of the isolated Cu^{2+} ion was $g_\parallel = 2.39$–2.40 for ideal octahedral coordination and decreased gradually with decreasing coordination to $g_\parallel = 2.32$–2.30 for fourfold quadratic coordination.

It is noteworthy that ESR spectra of Cu^{2+} ions with $g_\perp > g_\parallel > g_e$ have been observed rarely. A model to describe them was proposed for the first time in (17). The ESR lines were attributed to clusters of four interconnected quadratic-coordinated axially symmetrical Cu^{2+} ions in the ground state $d_{x^2-y^2}$ with tetragonal axes lying in the cluster plane and being perpendicularly correlated. In this model, the following relations can be written for the ESR spectrum of the cluster:

$$g_\parallel = g_1 \qquad [1]$$

$$g_\perp = (g_2 + g_3)/2, \qquad [2]$$

where $g_1 = g_2$ are the perpendicular components and g_3 is the parallel component of the *g* tensor of the isolated axially symmetrical Cu^{2+} complexes from which the cluster is built.

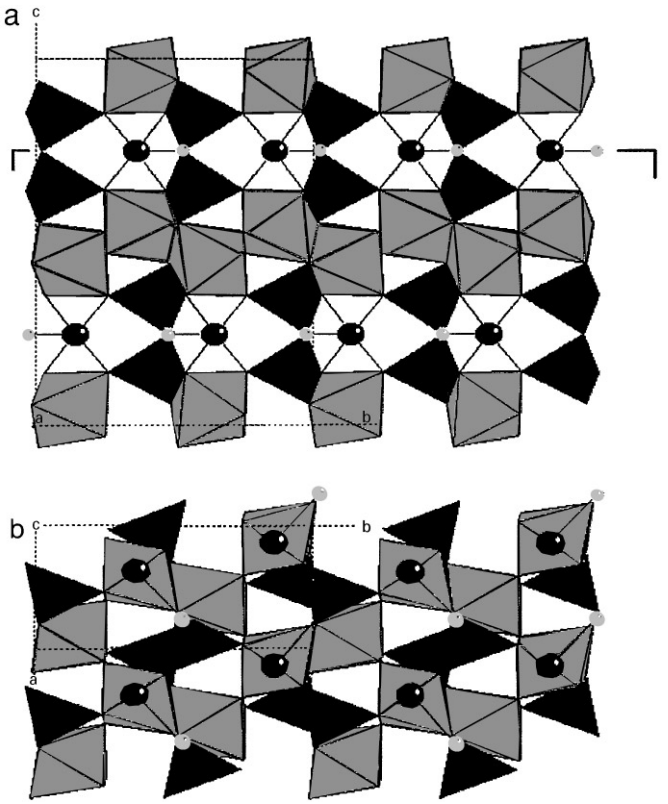

FIG. 10. Cualsite structure projected down x (a) and down z (b) to show the zigzag $[CuO_4]$ chains (the very top polyhedra are removed in b to make Cu atoms visible).

As will be shown in a separate paper, relations [1] and [2] are fulfilled satisfactorily if an exchange interaction exists between cooperatively ordered Cu^{2+} ions (e.g., –Cu–O–Si–O–Cu–) in their ground state $d_{x^2-y^2}$, which is the case in cualsite, where one can separate the zigzag chains of $[CuO_4]$ squares (the zigzag angle being 103°, which is close enough to 90°) directed along the b axis (Figs. 10a and 10b). When two neighboring $[CuO_4]$ squares are perpendicular to one another, one can easily obtain

$$g_a = g_b = g_\perp = (g_2 + g_3)/2 \qquad [3]$$

$$g_\parallel = g_c = g_1. \qquad [4]$$

Ignoring weak distortions of $[CuO_4]$ complexes, we can assume that $g_1 = g_2$ and obtain $g_3 = 2g_a - g_c = 2.35$ from [3] and [4]. This value corresponds well to the distorted octahedral (up to fivefold pyramidal) oxygen surroundings of the Cu^{2+} ion. Thus the main ESR spectrum of cualsite is described fairly well by the above model of the infinite zigzag chains.

In addition to the main ESR line, an isotropic spectrum of low intensity was observed in the region connected to double-quantum transitions ($g = 4.2$–4.3). It consisted of a few lines of various intensities with hyperfine splitting (HFS) corresponding to a HFS value $A_0 = 35$ Oe. They may be associated with isolated dimers of Cu^{2+} ions. Unfortunately, because of the strong ESR lines of the main ESR spectrum, it was impossible to isolate the fine-structure spectrum, which corresponds to formation of dimers with $S = 1$. The presence of dimers may be due to some irregularities of the cualsite lattice and/or incorporation of some Cu-substituting atoms (or vacancies) into the chain followed by breaking of exchange bonds between Cu ions. The low isotropic HFS value may be due to the opposite signs of the main A tensor components $A_\perp$ and $A_\parallel$.

DISCUSSION

Cualsite, $CuAl_2Si_2O_7(F,OH)_2$, is a new member of a copper silicate family with relatively few members, comprising both natural and synthetic compounds. From the chemical point of view, its chemical composition, method of synthesis (growth on topaz), and crystal structure allow one to consider cualsite as a copolymer of topaz ($Al_2[SiO_4](F, OH)_2$) and a hypothetical copper metasilicate, $CuSiO_3$. Nevertheless, contrary to most known copper silicates, cualsite contains no chains or other infinite silicate units. $[Si_2O_7]$ diortho groups are isolated in the cualsite structure and form together with $[CuO_5]$ polyhedra some kind of layers in the *ab* plane (Fig. 6). These layers are sandwiched between layers of $[AlO_4F_2]$ octahedra, which are fully identical to those existing in the topaz structure (Figs. 7b and 7e). This is the main reason for the observed over- and intergrowth of cualsite and topaz perpendicular to the c axis.

Denoting the $[AlO_4F_2]$ octahedral layers by O and $[SiO_4]$ tetrahedra by T, we can write for topaz the following sequence: $\{–O–T–O–T–\}_\infty$. By analogy, we can write $\{–O–T–Cu–T–O–\}_\infty$ for cualsite, where Cu denotes $[CuO_{4+1}]$ pyramids. Due to the almost full identity of both structures in *ab* plane formation, various intermediate combinations of these layers seem possible. For example, $\{–O–T–O–T–Cu–T–O–T–\}_\infty$ or some other combination of layers may exist, depending primarily on the chemical composition of the crystallization medium. In this case, the following general formula may be written: $x CuSiO_3 \cdot Al_2[SiO_4](F, OH)_2$, where $0 < x \leq 1$. Such compositional variability is characteristic for the copolymers and can explain the anomalously low Cu content in blue zones on the topaz seeds, which were grown under Cu-deficient conditions.

The perfect $\{001\}$ cleavage found in cualsite is of the same nature as that in topaz (13). It is easy to see in Fig. 7 that the weak directions of Al–O and Al–F bond rupture (dashed lines) are preserved in cualsite and are responsible for this cleavage.

As discussed in the previous section, coordination polyhedra and interatomic distances and angles in cualsite coincide fairly well with known correlations and are of the same magnitude as in other copper silicates. The Cu^{IV}–O distance for approximately square coplanar coordination varies normally from 1.932 Å in $Li_2Cu_5(Si_2O_7)_2$ (7) to 1.995 Å in $Cu_5(SiO_3)_4(OH)_2$ (1), being 1.96(1) Å for Cu^{IV} in (IV + I) coordination (7). In cualsite, these distances are 1.946 and 1.955 Å. The fifth Cu–O distance in the square pyramid is always larger and varies from 2.240 Å in $Ca_2Cu_2Si_3O_{10} \cdot 2H_2O$ (3) to 2.692 Å in $Cu_5(SiO_3)_4(OH)_2$ (1). In cualsite, the fifth Cu–O distance is 2.366 Å. It is noteworthy that this vertex (fifth) oxygen is at the same time a bridging oxygen of the Si_2O_7 group (Fig. 8). Its participation in both the (CuO_{4+1}) pyramid and the Si_2O_7 diortho group may result in an abnormally small Si–O–Si angle (123.7° compared to an average value 139° (15)).

A very similar arrangement of coordination polyhedra was observed in the mineral papagoite, $Ca_2Cu_2Al_2[Si_4O_{12}](OH)_6$ (5), where Cu^{2+} is also in a plane formed by edges of two [AlO_6] octahedra. $(Cu–O)_{av} = 1.95$ Å and the Cu to fifth oxygen atom distance is 2.402 Å. Similar to the arrangement in cualsite, the [AlO_6] octahedra in papagoite are also connected by [Si_2O_7] diortho groups (or more precisely by [Si_4O_{12}] rings), but contrary to cualsite, the bridging oxygen, though it was included in Cu^{2+} coordination in (5), is too far from Cu^{2+} and the ⟨Si–O–Si⟩ angle = 138.14°, which is very close to the average value 139°.

A distinct covalent component of the Cu–O bond is confirmed by ESR measurements. The ESR spectrum of cualsite reflects an exchange interaction of Cu^{2+} ions arranged in an infinite zigzag chain along the *b* axis.

The larger isomorphic capacity of cualsite compared to that of topaz is easily understandable in terms of their structures. The topaz structure is based on the oxygen (and fluorine) close packing and almost all [AlO_4F_2] octahedra have common O–O edges, whereas the cualsite structure is much more open and flexible. This helps to compensate and/or to relax any possible deformations which may arise during V substitution for Al, which was obtained in our hydrothermal experiments.

CONCLUSION

The single-crystal structure of a new copper aluminum silicate $CuAl_2Si_2O_7(F,OH)_2$ (cualsite) synthesized hydrothermally was determined and was shown to be in close relation to that of topaz. Full identity between both structures in the *ab* plane explains well the epitaxial overgrowth of cualsite on the topaz single-crystal seeds.

The physical properties of cualsite coincide well with its structure, in which the topaz layered fragments alternate with the [$CuSiO_3$] layers in the [001] direction. Copper coordination is a (4 + 1) square pyramid with a vertex oxygen being the bridging oxygen of the [Si_2O_7] diortho group. Zigzag chains (with intrachain angle 103°) formed by [CuO_4] squares inside [$CuSiO_3$] layers coincide well with the ESR spectrum of interacting Cu^{2+} in cualsite.

The main interatomic distances and angles in cualsite fall in the range typical for other known copper silicate structures. The only exception is a very small diortho groups Si–O–Si angle (123.7°).

ACKNOWLEDGMENTS

The authors are indebted to Dr. V. A. Gritchin from Novosibirsk State Technical University for piezoelectric measurements and Prof. V. F. Anufrienko for fruitful discussion of ESR results.

REFERENCES

1. H. T. Evans, Jr. and M. E. Mrose, *Am. Mineral.* **62,** 491 (1977).
2. K. Kawamura and K. Kawahara, *Acta Crystallogr., Sect. B* **32,** 2419 (1976).
3. R. B. Laughon, *Am. Mineral.* **56,** 193 (1971).
4. J. M. M. Pozas, G. Rossi, and V. Tazzoli, *Am. Mineral.* **60,** 471 (1975).
5. L. A. Groat and F. C. Hawthorne, *Mineral. Petrol.* **37,** 89 (1987).
6. K. Kawamura and A. Kawahara, *Acta Crystallogr.*, Sect. B **33,** 1071 (1977).
7. K. Kawamura, A. Kawahara, and J. T. Iiyama, *Acta Crystallogr., Sect. B* **34,** 3181 (1978).
8. K. A. Alexandrov and B. V. Beznosikov, "Perovskite Type Octahedral Crystals." Nauka, Novosibirsk, 1996.
9. M. S. Lehmann and F. K. Larsen, *Acta Crystallogr., Sect. A* **30,** 580 (1974).
10. G. M. Sheldrick, SHELXS-90. Program for Solving Crystal Structures, Univ. Goettingen, Goettingen, 1990.
11. G. M. Sheldrick, SHELXL-93. Program for Refinement of Crystal Structures, Univ. Goettingen, Goettingen, 1993.
12. "Minerals: Silicates with Single and Double Tetrahedra," Vol. IIIa, pp. 274–290. Nauka, Moscow, 1972.
13. P. H. Ribbe and P. E. Rosenberg, *Am. Mineral.* **56,** 1812 (1971).
14. P. H. Ribbe and G. V. Gibbs, *Am. Mineral.* **56,** 24 (1971).
15. F. Liebau, "Structural Chemistry of Silicates," Springer, Berlin, 1985.
16. S. A. Al'tshuler and B. M. Kozyrev, "Electronic Paramagnetic Resonance of Intermediate Group Element Compounds," Nauka, Moscow, 1972.
17. D. Reinen and C. Friebel, *Struct. Bonding* **37,** 1 (1979).
18. P. H. Ribbe and P. E. Rosenberg, *Am. Mineral.* **56,** 1812 (1971).